Thermodynamics of Chain Fluids from Atomistic Simulation: A Test of the Chain Increment Method for Chemical Potential

Theodora Spyriouni,[†,‡] Ioannis G. Economou,[†] and Doros N. Theodorou*[,†,‡]

Molecular Modelling of Materials Laboratory, Institute of Physical Chemistry, National Research Centre for Physical Sciences "Demokritos", GR 15310 Ag. Paraskevi Attikis, Greece, and Department of Chemical Engineering, University of Patras, GR 26500 Patras, Greece

Received February 7, 1997; Revised Manuscript Received May 5, 1997[⊗]

ABSTRACT: A formulation is presented for the calculation of the excess chemical potential $\mu^{ex}(n_{test})$ of n_{test}-mer chains mixed at infinite dilution with a bulk n-mer fluid and of the excess segmental chemical potential $\mu^{ex}_{seg} = \mu^{ex}(n+1) - \mu^{ex}(n)$ from detailed atomistic simulations. The formulation is applied for $n_{test} = 6$ to 16 in n-hexadecane (C_{16}, $n = 16$) in the liquid ($P = 50$ atm) and vapor ($P = 1.02$ atm) states at $T = 580$ K using a configurational bias Monte Carlo (MC) scheme. Two different reference states (ideal gas and continuous unperturbed chains) are examined for the definition of μ^{ex}, and simulations are conducted with two united-atom model representations from the recent literature. In parallel, μ^{ex} and μ^{ex}_{seg} with reference to the ideal gas are derived from two cubic equations of state (EoS) for the same systems and conditions. Both the MC and the EoS calculations for both models and reference states examined give a linear dependence of $\mu^{ex}(n_{test})$ on n_{test}, confirming that chemical potentials for long chains can be reliably estimated from small test chain and test segment insertions. This confirmation of the "chain increment ansatz" is of great practical value for phase equilibrium calculations in long-chain systems. Predictions for the structure of the C_{16} liquid and vapor are in good agreement with existing experimental and simulation evidence. Chain conformations in the liquid and vapor are indistinguishable from unperturbed and ideal gas chain conformations, respectively. In lower temperature liquids ($T =$ 450 K, $P = 20$ atm), insertions of long test chains cannot provide adequate sampling, but the chain increment ansatz remains useful for estimating chemical potentials.

1. Introduction

The use of polymers in many technological applications has resulted in a growing need for accurate knowledge of their thermophysical, rheological, mechanical, optical, and other properties. Experimental data for many of these properties are often unavailable because of practical difficulties (extreme conditions, degradation of polymers, etc.). On the other hand, the increase in computing power over the last decade provided the capability for simulating realistic polymer systems at the molecular level. Through such simulations, the properties of interest can be estimated reliably and a thorough understanding can be gained of the fundamental principles that control these properties.[1]

Thermodynamic properties and phase equilibria of polymer systems are of particular interest to polymer industry. An efficient design of a polymer process relies, *inter alia*, on the accurate estimation of the conditions that ensure complete miscibility of the polymer with a solvent during polymerization or flow through processing equipment and partial miscibility during separation or product formation. Calculation of the phase equilibria for small and nonpolar molecules (for example, C_1 to C_6 hydrocarbons) does not pose great difficulties if the intermolecular potentials are accurately known.[2,3] Unfortunately, many of the traditional techniques developed for small molecules (such as canonical, isothermal−isobaric, grand canonical, and Gibbs ensemble[4] Monte Carlo simulation) fail when applied to polymers. These techniques require the insertion or transfer of a molecule of the species whose chemical potential is calculated, imposed, or equalized between two phases, and this insertion or transfer has a very low statistical weight or probability of success because of the high density and size of polymer molecules. As a result, alternative ways need to be developed for the calculation of the chemical potentials of polymers.

Kumar *et al.*[5] proposed the so-called chain increment method. This relies on the ansatz that an appropriately defined excess chemical potential for a long n-mer chain in a bulk phase is a linear function of the chain length n for sufficiently long n and can therefore be expressed as

$$\mu^{ex}(n) = \mu^{ex}(n_{small}) + (n - n_{small})\,\mu^{ex}_{seg} \qquad (1)$$

where $\mu^{ex}(n_{small})$ is the chemical potential of an oligomer, for which Widom insertions[6] can readily be performed in the bulk phase, and μ^{ex}_{seg} is an appropriately defined excess segmental chemical potential, obtainable through a virtual process of augmenting a chain by one segment. We will refer to eq 1 as the "chain increment ansatz". If it holds, it can reduce the computational effort for performing phase equilibrium simulations in polymeric systems very substantially, for it reduces the problem of Widom insertion of a polymer chain into the bulk system to the much simpler problems of Widom insertion of a short oligomer and virtual addition of a segment to an existing chain. The chain increment ansatz has been tested[5] and widely implemented for simple, idealized models.[7,8] An early investigation by de Pablo *et al.*,[9] using a realistic united atom model for normal alkanes, indicated that the linearity of eq 1 is not fulfilled, at least up to n-decane. More recently, however, the ansatz has been invoked in phase equilibrium calculations with realistic models of stiff chains.[10]

Various strategies have been used for the estimation of chemical potentials of long chains from a simulation.

* Author to whom correspondence should be addressed at the University of Patras. Phone: +3061-997-398. FAX: +3061-993-255. E-mail: doros@sequoia.iceht.forth.gr.
[†] National Research Centre for Physical Sciences "Demokritos".
[‡] University of Patras.
[⊗] Abstract published in *Advance ACS Abstracts,* July 1, 1997.

S0024-9297(97)00178-2 CCC: $14.00

Escobedo and de Pablo[11] developed an expanded ensemble whose states correspond to different chain lengths of a tagged molecule, wherein the chemical potential is calculated from the contributions of the various states of the system. Müller and Paul,[12] Wilding and Müller,[13] and Wolfgardt *et al.*[14] proposed related methods. The idea behind these methods is the gradual insertion of a "ghost" polymer, using a parameter that controls the interactions between the inserted chain and the host phase.

In recent years, theoretical and semitheoretical analytical approaches have been proposed for the calculation of thermodynamic properties and phase equilibria of polymer systems. Some of these approaches invoke approximations related to the chain increment ansatz. Hall and co-workers[15,16] developed the generalized Flory dimer (GFD) theory, which estimates the equation of state of chain molecules from the equation of state of monomers and dimers that comprise the chain. Chapman *et al.*[17] developed the statistical associating-fluid theory (SAFT), based on the first-order thermodynamic perturbation theory (TPT-1) of Wertheim.[18,19] SAFT has been applied to a variety of homopolymer and copolymer systems.[20,21] Using a similar approach, Prausnitz and co-workers[22] proposed the perturbed-hard-sphere−chain (PHSC) equation of state, which was used to correlate experimental data for polymer mixtures and blends. All these models contain a number of adjustable parameters, and so fitting is required for quantitative agreement with experimental data.

The present work has been carried with the following objectives in mind. (a) The first is to develop a rigorous formulation for calculating the excess chain chemical potential μ^{ex} and the excess segmental chemical potential μ^{ex}_{seg} from detailed atomistic simulations of a chain fluid. Particular emphasis is laid on the role of bond angle bending, torsional potentials, and constant bond length constraints in the resulting expressions. (b) The second is to test whether the values μ^{ex} and μ^{ex}_{seg} obtained from well-converged atomistic simulations of a chain fluid in the liquid and vapor states conform to the chain increment ansatz (eq 1) and to determine the minimum acceptable value of n_{small} that can be used in it. Since the chain conformation in the liquid state is known to be close to unperturbed (compare ref 23), liquid state chemical potentials are computed with reference to both the ideal gas and unperturbed chains, and the validity of the incremental ansatz is examined for both reference states. (c) The third is to calculate chain and segmental chemical potentials from macroscopic equations of state which are known to give results in excellent agreement with experiment for the systems and conditions examined. Examination of these EoS predictions in conjunction with eq 1 allows us to judge, for the first time, whether the chain increment ansatz is in agreement with the real-life thermodynamic behavior of linear hydrocarbons. On the other hand, comparisons between EoS and simulation results give us a measure of how adequate the model representations invoked in the simulations are for capturing phase equilibria in these systems. (d) The last is to examine simulation predictions for the density, cohesive energy, inter- and intramolecular structure, and chain conformation in the chain liquid and gas in the light of existing evidence from past experimental and simulation work.

We have chosen a heavy normal alkane, *n*-hexadecane (C_{16}), as our test system. This is admittedly much shorter than the polymeric systems in whose phase equilibria we are mainly interested in. Nevertheless, this choice affords performing well-equilibrated simulations without excessive computational effort and makes use of very accurate EoS, which are not available for longer-chain systems. Excess chemical potentials have been calculated for *n*-hexane to *n*-pentadecane at infinite dilution in C_{16} and for the C_{16} chains themselves. A subcooled liquid state ($P = 50$ atm) and a superheated vapor state ($P = 1.02$ atm) of C_{16} have been examined, both at $T = 580$ K ($T_r = T/T_c = 0.8$). In addition, a lower-temperature subcooled liquid state ($P = 20$ atm, $T = 450$ K, $T_r = T/T_c = 0.6$) has been examined.

This paper is organized as follows. Section 2 is a brief overview of the molecular models used in the simulations. The theoretical formulation for the excess chain and segmental chemical potentials is developed in the first two parts of section 3, where the configurational bias MC integration strategy used to obtain these chemical potentials from *NPT* MC simulations of the C_{16} fluid is also explained. The third part of section 3 contains a brief discussion of equations of state and how they are used to calculate the chemical potentials of interest. Some technical details of the MC simulations conducted are given in section 4. Results on the volumetric behavior, structure, and conformation of the C_{16} liquid and vapor are presented in the first part of section 5. Results on the excess chemical potentials and comparisons against the chain increment ansatz are given in the second part of the same section. Finally, section 6 summarizes some important points.

2. Molecular Models

Several potential models have been proposed for long-chain alkanes. In the present work, two united atom potential representations, designed to mimic the behavior of real molecules, are employed. The first one was used by Dodd and Theodorou[23] for the prediction of volumetric and structural properties of *n*-tetracosane (*n*-C_{24}) and *n*-octaheptacontane (*n*- C_{78}) at various pressures at 450 K. The second potential was developed by Smit *et al.*[24] to calculate the vapor−liquid equilibria of several normal alkanes up to *n*-octatetracontane (*n*-C_{48}) near their critical points. In both these past sets of simulations, good agreement with experiment was obtained.

Both models use the Lennard−Jones potential to account for nonbonded inter- and intramolecular interactions and a continuous torsional potential. Bond lengths are kept fixed at 1.54 Å. The Dodd and Theodorou model uses fixed bond angles, while the Smit *et al.* model uses flexible bond angles. Finally, the Dodd and Theodorou model uses the same Lennard−Jones parameters for both the end and internal segments in a chain, whereas the Smit *et al.* model assigns much higher values to the energy parameter ϵ of the end segments. This differentiation of the end segment energy is believed[24] to compensate for the implicit representation of the hydrogens, especially at high densities.

In Table 1 we give an analytical description of the two models.

In all cases, the pair potential is truncated at $r = 2.3\sigma$ and its first and second derivatives are set to zero for $r > 2.3\sigma$. A quintic spline is used between $r = 1.45\sigma$ and $r = 2.3\sigma$ to eliminate discontinuities associated with the truncation.[25] Tail corrections are taken into account in all simulations by direct integration.[2]

The single chains simulated to obtain the properties of the two reference systems considered in this work are

Table 1. Atomistic Molecular Models for *n*-alkanes

Type of interaction	*Potential function and parameters*	
	Dodd and Theodorou model[23]	Smit *et al.* model[24]
Non bonded interactions	$U_{LJ}(r_{ij}) = 4\epsilon[(\sigma_{ij}/r_{ij})^{12} - (\sigma_{ij}/r_{ij})^{6}]$	
	$\epsilon_{CH_3}/k_B = \epsilon_{CH_2}/k_B = 49.3$ K $\sigma_{CH_3} = \sigma_{CH_2} = 3.94$ Å	$\epsilon_{CH_3}/k_B = 114$ K $\epsilon_{CH_2}/k_B = 47$ K $\sigma_{CH_3} = \sigma_{CH_2} = 3.93$ Å
Bond bending	Fixed angles $\theta_{fixed} = 112^o$	$U_{bending}(\theta)/k_B = 1/2k_\theta(\theta - \theta_{eq})^2$ $k_\theta = 62,500$ Krad^{-2} $\theta_{eq} = 114^o$
Dihedral angles	$U_{tors}(\phi)/k_B = \sum_{k=0}^{5} c_k \cos^k(\phi)$ $c_0 = 1116$ K, $c_1 = 1462$ K, $c_2 = -1578$ K, $c_3 = -368$ K, $c_4 = 3156$ K, $c_5 = -3788$ K	$U_{tors}(\phi)/k_B = c_1(1 + \cos\phi) + c_2(1 - \cos(2\phi)) + c_3(1 + \cos(3\phi))$ $c_1 = 355.03$ K $c_2 = -68.19$ K $c_3 = 791.32$ K

governed by the same potentials as chains in the bulk phases. *Ideal gas chains* retain all bonded and nonbonded intramolecular interactions along their contour. *Continuous unperturbed chains*, on the other hand, are unperturbed by nonlocal (long range) interactions; more specifically, nonbonded interactions between segments separated by more than four bonds along the backbone are omitted in sampling continuous unperturbed chains.[23]

3. Theory

Excess Chemical Potential of Chains from Simulations in the *NPT* Ensemble. In our investigations of the chain increment ansatz we will be concerned with a chain of n_{test} segments or mers (*i.e.*, methyl or methylene units) at infinite dilution within a fluid of n-mer chains at temperature T and pressure P. The chemical potential (partial molecular Gibbs energy) of such a chain can be obtained from the following difference in the thermodynamic limit $N \to \infty$

$$\beta\mu(T,P) = -\ln Q_P(N;n,1;n_{test},P,T) + \ln Q_P(N;n,P,T) = -\ln\frac{\int dV \exp(-\beta PV)Q(N;n,1;n_{test},V,T)}{\int dV \exp(-\beta PV)Q(N;n,V,T)} = -\ln\frac{\int dV \exp(-\beta PV)Q(N;n,V,T)\dfrac{Q(N;n,1;n_{test},V,T)}{Q(N;n,V,T)}}{\int dV \exp(-\beta PV)Q(N;n,V,T)} = -\ln\left\langle\frac{Q(N;n,1;n_{test},V,T)}{Q(N;n,V,T)}\right\rangle_{NPT} \quad (2)$$

where $Q_P(N;n,1;n_{test},P,T)$ stands for the isothermal−isobaric partition function of a system of N n-mer chains and one n_{test}-mer chain at P and T, and $Q_P(N;n,P,T)$ is the isothermal−isobaric partition function for a system of N n-mer chains at P and T. $Q(N;n,1;n_{test},V,T)$ and $Q(N;n,V,T)$ are the corresponding canonical partition functions at volume V and temperature T. The subscript NPT on the right-hand side of eq 2 denotes that fluctuations in volume are sampled according to the isothermal−isobaric ensemble for N n-mer chains at P and T.

We will symbolize by Λ the thermal wavelength of the segments (assumed here of equal mass, without loss of generality), by $U(\mathbf{r},\mathbf{r}_{test};N;n,1;n_{test})$ the potential energy function of a system of N n-mer chains and one n_{test}-mer chain, and by $U(\mathbf{r};N;n)$ the potential energy function of a system of N n-mer chains. The $3Nn$-dimensional vector $\mathbf{r}$ comprises the Cartesian coordinates of all segments of all n-mer chains, while the $3n_{test}$-dimensional vector $\mathbf{r}_{test}$ consists of the coordinates of all segments of the n_{test}-mer chain, of which the first three correspond to overall translation of the chain. The ratio of canonical partition functions on the right-hand side of eq 2 becomes

$$\frac{Q(N;n,1;n_{test},V,T)}{Q(N;n,V,T)} = \frac{\frac{1}{N!\Lambda^{3(Nn+n_{test})}}\int d^{3Nn}r\int d^{3n_{test}}r_{test}\exp[-\beta U(\mathbf{r},\mathbf{r}_{test};N;n,1;n_{test})]}{\frac{1}{N!\Lambda^{3Nn}}\int d^{3Nn}r\exp[-\beta U(\mathbf{r};N;n)]} = \frac{1}{\Lambda^{3n_{test}}}\times\frac{\int d^{3Nn}r\int d^{3n_{test}}r_{test}\exp[-\beta U(\mathbf{r};N;n)]\exp[-\beta U_{test}(\mathbf{r}_{test};\mathbf{r};N;n)]}{\int d^{3Nn}r\exp[-\beta U(\mathbf{r};N;n)]} \quad (3)$$

On the right-hand side of eq 3 we have defined the "test"-energy of the n_{test}-mer chain as the difference

$$U_{test}(\mathbf{r}_{test};\mathbf{r};N;n) = U(\mathbf{r},\mathbf{r}_{test};N;n,1;n_{test}) - U(\mathbf{r};N;n) \quad (4)$$

The domain of integration for all coordinates is the volume V.

We will compare the chemical potential $\mu(T,P)$ to that of a n_{test}-mer chain in a reference system containing one n_{test}-mer chain and N n-mer chains at temperature T and density $\rho = N/\langle V\rangle_{NPT}$, equal to that of the system of interest. As mentioned in sections 1 and 2, the reference system is chosen as either an ideal gas or as a system of noninteracting unperturbed chains. By definition, the potential energy of this reference system is a sum of independent intramolecular terms. Through a development entirely analogous to that leading to eq 3, we obtain

$$\beta\mu_{ref}(T,\rho) = -\ln\left[\frac{Q_{ref}(N;n,1;n_{test},\langle V\rangle_{NPT},T)}{Q_{ref}(N;n,\langle V\rangle_{NPT},T)}\right] = -\ln\left[\frac{\langle V\rangle_{NPT}}{\Lambda^{3n_{test}}}\times\frac{\int d^{3Nn}r\int d^{3n_{test}-3}r_{test}'\exp[-\beta U_{ref}^{tot}(\mathbf{r};N;n)]\exp[-\beta U_{ref}(\mathbf{r}_{test})]}{\int d^{3Nn}r\exp[-\beta U_{ref}^{tot}(\mathbf{r};N;n)]}\right] \quad (5)$$

where $U_{ref}(\mathbf{r}_{test})$ is the energy of a single reference chain in configuration $\mathbf{r}_{test}$. In eq 5, $\exp[-\beta U_{ref}^{tot}(\mathbf{r};N,n)]$ can be factored into N terms, each depending only on the coordinates of a single n-mer chain. Thus, the integrals over $\mathbf{r}$ in the numerator and denominator of eq 5 cancel, leading to

$$\beta\mu_{ref}(T,\rho) = -\ln\left\{\frac{\langle V\rangle_{NPT}}{\Lambda^{3n_{test}}}\int d^{3n_{test}-3}r_{test}'\exp[-\beta U_{ref}(\mathbf{r}_{test}')]\right\} \quad (6)$$

In eqs 5 and 6, the integration over the three translational degrees of freedom of the test chain has been carried out, leading to the $\langle V\rangle_{NPT}$ term. The symbol $\mathbf{r}_{test}'$ will be used to denote the remaining (nontranslational) part of $\mathbf{r}_{test}$.

Substituting eq 3 in eq 2 and subtracting eq 6 from the result, one obtains

$$\beta\mu^{\mathrm{ex}} \equiv \beta\mu - \beta\mu_{\mathrm{ref}} = -\ln\left[\frac{1}{\langle V\rangle_{NPT}} \times \left\langle \frac{\int \mathrm{d}^{3Nn} r \int \mathrm{d}^{3n_{\mathrm{test}}} r_{\mathrm{test}} \exp[-\beta U(\mathbf{r};N;n)] \exp[-\beta U_{\mathrm{test}}(\mathbf{r}_{\mathrm{test}};\mathbf{r};N;n)]}{\int \mathrm{d}^{3Nn} r \exp[-\beta U(\mathbf{r};N;n)] \int \mathrm{d}^{3n_{\mathrm{test}}-3} r_{\mathrm{test}}{}' \exp[-\beta U_{\mathrm{ref}}(\mathbf{r}_{\mathrm{test}}')]} \right\rangle_{NPT}\right] \quad (7)$$

Multiplying and dividing the argument of the logarithm in eq 7 by $\int \mathrm{d}^{3n_{\mathrm{test}}-3} r_{\mathrm{test}}{}'$

$$\beta\mu^{\mathrm{ex}} = -\ln\left[\frac{1}{\langle V\rangle_{NPT}} \times \left\langle \frac{\int \mathrm{d}^{3Nn} r \int \mathrm{d}^{3n_{\mathrm{test}}} r_{\mathrm{test}} \exp[-\beta U(\mathbf{r};N;n)] \exp[-\beta U_{\mathrm{test}}(\mathbf{r}_{\mathrm{test}};\mathbf{r};N;n)]}{\int \mathrm{d}^{3Nn} r \exp[-\beta U(\mathbf{r};N;n)] \int \mathrm{d}^{3n_{\mathrm{test}}-3} r_{\mathrm{test}}{}'} \right\rangle_{NPT}\right] + \ln\left(\frac{\int \mathrm{d}^{3n_{\mathrm{test}}-3} r_{\mathrm{test}}{}' \exp[-\beta U_{\mathrm{ref}}(\mathbf{r}_{\mathrm{test}}')]}{\int \mathrm{d}^{3n_{\mathrm{test}}-3} r_{\mathrm{test}}{}'}\right) = -\ln\left[\frac{1}{\langle V\rangle_{NPT}} \times \left\langle V \frac{\int \mathrm{d}^{3Nn} r \int \mathrm{d}^{3n_{\mathrm{test}}} r_{\mathrm{test}} \exp[-\beta U(\mathbf{r};N;n)] \exp[-\beta U_{\mathrm{test}}(\mathbf{r}_{\mathrm{test}};\mathbf{r};N;n)]}{\int \mathrm{d}^{3Nn} r \int \mathrm{d}^{3n_{\mathrm{test}}} r_{\mathrm{test}} \exp[-\beta U(\mathbf{r};N;n)]} \right\rangle_{NPT}\right] + \ln\left(\frac{\int \mathrm{d}^{3n_{\mathrm{test}}-3} r_{\mathrm{test}}{}' \exp[-\beta U_{\mathrm{ref}}(r_{\mathrm{test}}')]}{\int \mathrm{d}^{3n_{\mathrm{test}}-3} r_{\mathrm{test}}{}'}\right) = -\ln\left[\frac{1}{\langle V\rangle_{NPT}} \langle V \langle \exp(-\beta U_{\mathrm{test}})\rangle_{\mathrm{Widom}}\rangle_{NPT}\right] + \ln\langle \exp(-\beta U_{\mathrm{ref}})\rangle_{\mathrm{single\ chain}} \quad (8)$$

In the first term of eq 8, the inner (Widom) average refers to an n_{test}-mer chain inserted with random position, orientation, and conformation within a system of N n-mer chains in volume V, whose configuration is distributed according to the canonical ensemble at temperature T. The outer average requires that fluctuations of V be sampled according to the isothermal-isobaric ensemble at pressure P and temperature T. The average in the second term of eq 8 is taken over all conformations of a single chain, distributed according to the Boltzmann factor of the energy U_{ref}. We can rewrite eq 8 so as to show explicitly the role of inter- and intramolecular contributions to the two terms

$$\beta\mu^{\mathrm{ex}} = -\ln\left[\frac{1}{\langle V\rangle_{NPT}} \langle V \langle \exp(-\beta U_{\mathrm{test}}^{\mathrm{intra}} - \beta U_{\mathrm{test}}^{\mathrm{inter}})\rangle_{\mathrm{Widom}}\rangle_{NPT}\right] + \ln\langle \exp(-\beta U_{\mathrm{ref}}^{\mathrm{intra}})\rangle_{\mathrm{single\ chain}} \quad (9)$$

In the model representation employed here, bond lengths are considered to be governed by harmonic potentials whose spring constants tend to infinity (flexible model in the limit of infinite stiffness). By conversion to a set of generalized coordinates (chain start positions $\mathbf{r}_0$, Euler angles $\boldsymbol{\psi}$, bond lengths $\mathbf{l}$, bond angles $\boldsymbol{\theta}$, and torsion angles $\boldsymbol{\phi}$) the Boltzmann factors associated with the infinitely stiff bond length potentials give rise to δ functions in the bond length. Thus, configurational averages reduce to averages over $\mathbf{r}_0$, $\boldsymbol{\psi}$, $\boldsymbol{\theta}$, and $\boldsymbol{\phi}$ for each chain with the additional requirement of constant bond length, and the energies $U_{\mathrm{test}}^{\mathrm{intra}}$ and $U_{\mathrm{ref}}^{\mathrm{intra}}$ in eq 9 can be considered as devoid of any bond length contributions.[26]

Converting to generalized coordinates, an alternative expression for $\beta\mu^{\mathrm{ex}}$ is obtained from eq 7

$$\beta\mu^{\mathrm{ex}} = -\ln\left[\frac{1}{\langle V\rangle_{NPT}} \langle \int \mathrm{d}^{2n_{\mathrm{test}}+1} q_{\mathrm{test}} \exp(-\beta U_{\mathrm{test}}^{\mathrm{intra}} - \beta U_{\mathrm{test}}^{\mathrm{inter}})\rangle_{NPT}\right] + \ln[\int \mathrm{d}^{2n_{\mathrm{test}}-2} q_{\mathrm{test}}{}' \exp(-\beta U_{\mathrm{ref}}^{\mathrm{intra}})] \quad (10)$$

where $\mathbf{q} \equiv (\mathbf{r}_0,\boldsymbol{\psi},\boldsymbol{\theta},\boldsymbol{\phi})$, $\mathbf{q}' \equiv (\boldsymbol{\psi},\boldsymbol{\theta},\boldsymbol{\phi})$, and the volume elements $\mathrm{d}^{2n_{\mathrm{test}}+1} q_{\mathrm{test}}$, $\mathrm{d}^{2n_{\mathrm{test}}-2} q_{\mathrm{test}}{}'$ incorporate a Jacobian of transformation from Cartesian to generalized coordinates.[26] The configurational integrals in eq 10 are identical to those computed by Maginn *et al.* in the context of their study of low-occupancy sorption thermodynamics of alkanes in zeolites, the only difference being that, in the first term of eq 10, the test molecule insertion takes place not in a rigid porous framework but in a fluctuating matrix of n-mer chains, whose configurations are distributed according to the NPT ensemble.

Straightforward insertions of randomly oriented and conformed test chain molecules are much too inefficient for estimating the Widom average in eq 9, or the NPT-averaged configurational integral in eq 10. In this work we have adopted the configurational bias Monte Carlo integration (CBMCI) method of Maginn *et al.*[26] to both integrals in eq 10. The mathematical formulation underlying this method is developed in detail in ref 26 and will not be repeated here. We will only present the final expression, whereby μ^{ex} is calculated in the course of an NPT-simulation of the n-mer fluid

$$\beta\mu^{\mathrm{ex}} = -\ln\left\{\frac{1}{\langle V\rangle_{NPT}} \left\langle V \left\langle \frac{\exp(-\beta U_{\mathrm{test}}^{\mathrm{intra}} - \beta U_{\mathrm{test}}^{\mathrm{inter}})}{W_1} \right\rangle_{W_1} \right\rangle_{NPT} \times \Omega_{\mathrm{q}'} \frac{1}{N_{\mathbf{r}_0} N_{\psi_{12}} N_{\psi_3} N_{\theta_1} \cdots N_{\theta_{n_{\mathrm{test}}-2}} N_{\phi_2} \cdots N_{\phi_{n_{\mathrm{test}}-2}}}\right\} + \ln\left\{\left\langle \frac{\exp(-\beta U_{\mathrm{ref}}^{\mathrm{intra}})}{W_2} \right\rangle_{W_2} \times \Omega_{\mathrm{q}'} \frac{1}{N_{\mathbf{r}_0}{}' N_{\psi_{12}}{}' N_{\psi_3}{}' N'_{\theta_1} \cdots N'_{\theta_{n_{\mathrm{test}}-2}} N'_{\phi_2} \cdots N'_{\phi_{n_{\mathrm{test}}-2}}}\right\} \quad (11)$$

where the weights W_1 and W_2 are defined as follows

$$W_1 = \prod_{i=2}^{n_{\mathrm{test}}} \frac{\exp(-\beta U^{\mathrm{intra+inter}}(i))}{\sum_{j=1}^{n_{\mathrm{trial}}(i)} \exp(-\beta U^{\mathrm{intra+inter}}(i,j))}$$
$$W_2 = \prod_{i=4}^{n_{\mathrm{test}}} \frac{\exp(-\beta U_{\mathrm{ref}}^{\mathrm{intra}}(i))}{\sum_{j=1}^{n_{\mathrm{trial}}(i)} \exp(-\beta U_{\mathrm{ref}}^{\mathrm{intra}}(i,j))} \quad (12)$$

By $n_{\mathrm{trial}}(i)$ is denoted the number of trial positions j considered for the addition of each segment i of the chain. This equals $N_{\mathbf{r}_0}$ for placement of the first segment (chain start); $N_{\psi_{12}}$ for placement of the second segment; $N_{\theta_1} N_{\psi_3}$ for placement of the third, $N_{\theta_2} N_{\phi_2}$ for

placement of the fourth, and so on. The energy change associated with adding segment i in trial position j is symbolized by $U^{\text{intra+inter}}(i,j)$ for the test chain grown in the fluid and by $U_{\text{ref}}^{\text{intra}}(i,j)$ for the single reference chain. The corresponding values at the positions actually chosen in the course of the CBMCI procedure are $U^{\text{intra+inter}}(i)$ and $U_{\text{ref}}^{\text{intra}}(i)$, respectively. In the denominator of each ensemble average in eq 11 appears a product of the numbers $n_{\text{trial}}(i)$. $V\,\Omega_{q'}$ is the volume of configuration space for one chain

$$\Omega_{q'} = \int_0^{\pi}\sin\psi_1\,\mathrm{d}\psi_1\int_0^{2\pi}\mathrm{d}\psi_2\int_0^{2\pi}\mathrm{d}\psi_3\int_0^{\pi}\sin\theta_1\,\mathrm{d}\theta_1\times \int_0^{\pi}\sin\theta_2\,\mathrm{d}\theta_2\ldots\int_0^{\pi}\sin\theta_{n_{\text{test}}-2}\,\mathrm{d}\theta_{n_{\text{test}}-2}\int_0^{2\pi}\mathrm{d}\phi_2\times \int_0^{2\pi}\mathrm{d}\phi_3\ldots\int_0^{2\pi}\mathrm{d}\phi_{n_{\text{test}}-2} \quad (13)$$

In eq 11, $\Omega_{q'}$ is the same for chains generated in the bulk and for those generated to sample the reference states and thus cancels out. In the implementation used here, the start position of the test chain inserted in the n-mer fluid is selected randomly within the current volume of the simulation box (no bias for $\mathbf{r}_0$, $N_{\mathbf{r}_0} = 1$). For the reference chain, the positions of the two first segments are fixed ($N_{\mathbf{r}_{0'}} = N_{\psi_{12'}} = 1$), as is the plane of the first three segments ($N_{\psi 3'} = 1$). The values of $N_{\theta_i}(1 \le i \le n_{\text{test}} - 2)$ and $N_{\phi_i}(2 \le i \le n_{\text{test}} - 2)$ used for the test and the reference chain are discussed in section 4.

Excess Segmental Chemical Potential. Under given T and P, the segmental chemical potential μ_{seg} in a system of n-mer chains is defined as the change in total Gibbs energy brought about by replacing one n-mer chain in the system by an $(n+1)$-mer chain

$$\beta\mu_{\text{seg}}(T,P) = -\ln Q_{\text{p}}(N-1;n,1;n+1,P,T) + \ln Q_{\text{p}}(N;n,P,T) = -\ln\frac{Q_{\text{p}}(N-1;n,1;n+1,P,T)}{Q_{\text{p}}(N;n,P,T)} = -\ln\frac{\int \mathrm{d}V\exp(-\beta PV)Q(N-1;n,1;n+1,V,T)}{\int \mathrm{d}V\exp(-\beta PV)Q(N;n,V,T)} = -\ln\left\langle\frac{Q(N-1;n,1;n+1,V,T)}{Q(N;n,V,T)}\right\rangle_{NPT} \quad (14)$$

Clearly, in the thermodynamic limit one has

$$\beta\mu_{\text{seg}} = \beta\mu(n_{\text{test}} = n+1) - \beta\mu(n_{\text{test}} = n) \quad (15)$$

with $\mu(n_{\text{test}})$ defined by eq 2.

The ratio of canonical partition functions in eq 14 can be associated with a Widom process of appending an additional segment at the end of one of the chains of the original n-mer system. The appended segment experiences intramolecular interactions from its own chain and intermolecular interactions from the other chains. Note that there may be a change in intermolecular energy associated with converting what was previously an end segment of the augmented chain to an internal (penultimate) segment. The energy change associated with adding the segment to the n-mer system will be denoted as $U_{\text{seg}}(\mathbf{r}_{\text{seg}};\mathbf{r};N,n)$, with $\mathbf{r}_{\text{seg}}$ the position vector of the added segment and $\mathbf{r}$ the $3Nn$-dimensional vector describing the configuration of the n-mer system, as above. Then

$$\frac{Q(N-1;n,1;n+1,V,T)}{Q(N;n,V,T)} = \frac{N}{\Lambda^3}\times \frac{\int \mathrm{d}^{3Nn}r\int \mathrm{d}^3r_{\text{seg}}\exp[-\beta U(\mathbf{r};N;n)]\exp[-\beta U_{\text{seg}}(\mathbf{r}_{\text{seg}};\mathbf{r};N,n)]}{\int \mathrm{d}^{3Nn}r\exp[-\beta U(\mathbf{r};N;n)]} \quad (16)$$

If the same segment addition takes place in the reference system of noninteracting ideal gas or unperturbed n-mer chains at density $\rho = N/\langle V\rangle_{NPT}$, it will bring about a change in Helmholtz energy

$$\beta\mu_{\text{seg,ref}}(T,\rho) = -\ln Q_{\text{ref}}(N-1;n,1;n+1,\langle V\rangle_{NPT},T) + \ln Q_{\text{ref}}(N;n,\langle V\rangle_{NPT},T) = -\ln\left[\frac{N}{\Lambda^3}\frac{\int \mathrm{d}^{3Nn}r\int \mathrm{d}^3r_{\text{seg}}\exp[-\beta U_{\text{ref}}^{\text{tot}}(\mathbf{r};N;n)]\exp[-\beta U_{\text{seg,ref}}(\mathbf{r}_{\text{seg}};\mathbf{r};N,n)]}{\int \mathrm{d}^{3Nn}r\exp[-\beta U_{\text{ref}}^{\text{tot}}(\mathbf{r};N;n)]}\right] \quad (17)$$

But the total energy of the reference system consists of individual contributions $U_{\text{ref}}^{\text{intra}}$ from its noninteracting chains, so the ratio on the right-hand side of eq 17 can be simplified to a ratio of one-chain integrals over the degrees of freedom of the chain being augmented

$$\beta\mu_{\text{seg,ref}}(T,\rho) = -\ln\left[\frac{N}{\Lambda^3}\frac{\int \mathrm{d}^{3n}r_{\text{chain}}\int \mathrm{d}^3r_{\text{seg}}\exp[-\beta U_{\text{ref}}^{\text{intra}}(\mathbf{r}_{\text{chain}};n)]\exp[-\beta U_{\text{seg,ref}}^{\text{intra}}(\mathbf{r}_{\text{seg}};\mathbf{r}_{\text{chain}};n)]}{\int \mathrm{d}^{3n}r_{\text{chain}}\exp[-\beta U_{\text{ref}}^{\text{intra}}(\mathbf{r}_{\text{chain}};n)]}\right] \quad (18)$$

Owing to the stiff intramolecular potentials binding the added segment to its chain, the domain of $\mathbf{r}_{\text{seg}}$ contributing to the integrals in eqs 16 and 18 is confined to a small region of volume V_{seg} around the last segment of the augmented chain. For the potential models considered here, V_{seg} is the volume of an infinitesimally thin spherical shell of radius equal to the bond length l. The right-hand side of eq 18 is thus independent of $\langle V\rangle_{NPT}$. Upon subtracting eq 18 from eq 14, we obtain

$$\beta\mu_{\text{seg}}^{\text{ex}} = \beta\mu_{\text{seg}} - \beta\mu_{\text{seg,ref}} = -\ln\langle\int \mathrm{d}^3r_{\text{seg}}\exp(-\beta U_{\text{seg}}^{\text{intra}} - \beta U_{\text{seg}}^{\text{inter}})\rangle_{NPT} + \ln\langle\int \mathrm{d}^3r_{\text{seg}}\exp(-\beta U_{\text{seg,ref}}^{\text{intra}})\rangle_{\text{single chain}} \quad (19)$$

Adding and subtracting $\ln V_{\text{seg}}$, we can also write eq 19 as

$$\beta\mu_{\text{seg}}^{\text{ex}} = -\ln\langle\exp(-\beta U_{\text{seg}}^{\text{intra}} - \beta U_{\text{seg}}^{\text{inter}})\rangle_{\text{incr.},NPT} + \ln\langle\exp(-\beta U_{\text{seg,ref}}^{\text{intra}})\rangle_{\text{incr.,single chain}} \quad (20)$$

The first average on the right-hand side of eqs 19 and 20 corresponds to a procedure of incrementing one chain by one segment within a system of n-mer chains governed by the probability density distribution of the isothermal−isobaric ensemble. The second average corresponds to incrementing by one segment a single n-mer reference chain whose conformations are distributed according to the Boltzmann factor of $U_{\text{ref}}^{\text{intra}}$. As mentioned in conjunction with μ^{ex}, eqs 19 and 20 are readily recast in generalized coordinates, and bond length contributions to $U_{\text{seg}}^{\text{intra}}$ and $U_{seg,ref}^{\text{intra}}$ need not be included.

Again, the integrals on the right-hand side of eq 19 (particularly the first one) are best computed through

a configurational bias Monte Carlo scheme. Adapting the formalism of Maginn *et al.*[26] to this problem, we can write

$$\beta\mu_{\text{seg}}^{\text{ex}} = -\ln\left\{\left\langle\frac{\exp(-\beta U_{\text{seg}}^{\text{intra}} - \beta U_{\text{seg}}^{\text{inter}}}{W_{1\text{seg}}}\right\rangle_{W_{1\text{seg}},NPT} \times \Omega_{\text{qseg}}\frac{1}{N_{\text{seg}}}\right\} + \ln\left\{\left\langle\frac{\exp(-\beta U_{\text{seg}}^{\text{intra}})}{W_{2\text{seg}}}\right\rangle_{W_{2\text{seg}},\text{single chain}} \times \Omega_{\text{qseg}}\frac{1}{N_{\text{seg}}}\right\} \quad (21)$$

where the weights $W_{1\text{seg}}$ and $W_{2\text{seg}}$ are defined as follows

$$W_{1\text{seg}} = \frac{\exp(-\beta U_{\text{seg}}^{\text{intra+inter}}(i))}{\sum_{j=1}^{N_{\text{seg}}}\exp(-\beta U_{\text{seg}}^{\text{intra+inter}}(i,j))}$$

$$W_{2\text{seg}} = \frac{\exp(-\beta U_{\text{seg}}^{\text{intra}}(i))}{\sum_{j=1}^{N_{\text{seg}}}\exp(-\beta U_{\text{seg}}^{\text{intra}}(i,j))} \quad (22)$$

The notation is entirely analogous to that used in eq 12.

The volume Ω_{qseg} and the number of trial directions (N_{seg}) for putting the inserted segment cancel out in eq 21. In eqs 20 and 21, the single chain average is taken over *n*-mer chains that have been sampled according to $U_{\text{ref}}^{\text{intra}}$ by a Metropolis Monte Carlo algorithm. This is different from the procedure used for the single chain averages of eqs 8 and 11, where single chains are generated independently of each other.

Clearly, estimating the segmental chemical potential through biased Widom insertions of segments at the end of existing *n*-mer chains according to eq 21 is a computationally easier process than estimating the chain chemical potential through biased Widom insertions of entire chains according to eq 11.

Equation of State (EoS) Estimation of μ^{ex} and $\mu_{\text{seg}}^{\text{ex}}$. When ideal gas chains are used as a reference, the excess chemical potential can readily be obtained from a macroscopic description of the thermodynamics of mixtures of n_{test}-mer and *n*-mer chains, such as that provided by an equation of state. From its definition

$$\beta\mu^{\text{ex}} = \ln\phi^{\infty} + \ln\left(\frac{\beta P}{\rho}\right) \quad (23)$$

where ϕ^{∞} is the fugacity coefficient of n_{test}-mer chains at infinite dilution within an *n*-mer fluid at *T* and *P* and ρ is the molecular density of the *n*-mer fluid under these conditions. ϕ^{∞} is calculable from a mixture equation of state by standard methods.[27] In this work, two cubic equations of state were used for the description of *n*-hexadecane mixtures with shorter *n*-alkanes: The Soave−Redlich−Kwong (SRK) and the Peng−Robinson (PR). The parameters T_c, P_c, and ω for each component and the mixing and combining rules for these parameters were taken from refs 29 and 30. Estimates based on the SRK and PR equations for vapor−liquid equilibria of alkane mixtures in the range of molecular weights examined here are very accurate and can be considered as experimental information for all practical purposes.[27,28] Equation 23 was also used to calculate μ^{ex} for pure hexadecane, with ϕ^{∞} replaced by the fugacity coefficient ϕ, obtainable from the same equation of state for the pure fluid.

An estimate of $\mu_{\text{seg}}^{\text{ex}}$ is obtainable from macroscopic thermodynamics through

$$\beta\mu_{\text{seg}}^{\text{ex}} = \beta\mu^{\text{ex}}(n+1;n) - \beta\mu^{\text{ex}}(n) \quad (24)$$

where $\mu^{\text{ex}}(n+1;n)$ is the excess chemical potential of (*n*+1)-mer infinitely dilute in *n*-mer at *T* and *P*, and $\mu^{\text{ex}}(n)$ the excess chemical potential of pure *n*-mer, both estimated through eq 23.

4. Simulation Details

As mentioned in section 1, the system simulated here is pure *n*-C_{16} in the liquid and vapor states. The simulations were carried out with MC in the *NPT* ensemble, that is under constant temperature, pressure, and total number of molecules.

The numbers of chains simulated in the liquid and vapor phases were 32 and 8, respectively.

In both phases, the model system was equilibrated for about 5−10 million steps depending on the phase. The initial configuration was taken from a previously equilibrated chain liquid at lower temperature. Several quantities were checked during the run to ensure equilibration: First, the running average system pressure was calculated in the course of each run and compared to the imposed pressure. For this purpose, the "molecular virial" method[31] was used to obtain the pressure from intermolecular forces and distances. A second test of equilibration was based on chain conformational characteristics in the system. Quantities characterizing the overall size of chains are the radius of gyration($<s^2>$) and the mean squared end-to-end distance ($<r^2>$). Calculated values for these quantities were compared with the ideal gas and the continuous unperturbed chain estimates. Average values obtained from the vapor and liquid simulations are expected to compare well with the values calculated for ideal gas and unperturbed single chains, respectively, at the same temperature.

Production runs were about 30 million MC steps for each simulation in the bulk. Single-chain MC simulations to sample the reference states (ideal gas and unperturbed chains) were also conducted; these were much less computationally demanding than the bulk simulations. The MC moves used to sample the bulk chain fluid configurations in the *NPT* ensemble differed somewhat between liquid and vapor. For both phases, reptation, concerted rotation and volume fluctuation moves were used. In addition, rigid chain displacements were applied for the vapor phase, while in the liquid phase configurational bias (CB) moves were used.

In a rigid-chain displacement, one chain is selected and translated randomly to another position in the simulation box, without any change in its orientation or conformation. In the low-density vapor phase, this move had almost 100% acceptance rate, allowing the chains to move around the box, thus contributing to efficient sampling of the configuration space.

In a CB move[9,32−34] a randomly chosen chain is cut in two parts by severing a skeletal bond along its contour. One of the two parts is discarded and then regrown, segment by segment. At each step of this

regrowth procedure, a number of trial positions (n_{trial}) are considered for the added segment and one of these is chosen with a weight proportional to the Boltzmann factor of the energy increment associated with the addition. The bias associated with this procedure is removed in the selection criteria. The CB move is intimately related to the CBMCI procedure discussed in section 3 in conjunction with the estimation of chemical potentials. CB is particularly efficient for intermediate to high densities, especially for long molecules with internal stiffness. We used $n_{trial} = 6$. The acceptance rate of this move varied from 50% to 55%, the lower rate obtained with the Smit *et al.* model.

The reptation or "slithering snake" move involves randomly picking one end of a chain, deleting it, and appending a new segment at the other end. It was implemented as in refs 23 and 35. Its acceptance rate varied from 17% to 19% for the liquid and from 40% to 42% for the vapor phase. Again the lower rate was observed for the Smit *et al.* model. Although the chains in the vapor hardly see each other, the acceptance rate of this move does not even reach 50% because of the contracted conformations that the chains adopt in this phase.

The concerted rotation[35,36] (ConRot) move consists of a coordinated rotation of up to eight adjacent torsion angles along a chain that leaves the remainder of the chain unaffected. The symmetric, two-"driver angle" version of the move, sometimes termed "intramolecular rebridging",[35] was used here. In a flexible bond-angle model, such as that of Smit *et al.*, the bond angles may be kept fixed at their previous values or be rechosen during the move from a distribution proportional to $\sin\theta \exp(-\beta U_{bending}(\theta))$. The latter option was followed here. The acceptance rate was 15−27% for the liquid and 18−29% for the vapor phase, the lower rate again being observed for the Smit *et al.* model.

The volume fluctuation move applied in all *NPT* simulations was tuned, via the maximum allowed change in volume, to give an average acceptance rate of 50%.

The lower acceptance rate observed for the Smit *et al.* model in all cases is probably due to the high energetics of the end segments.

Single ideal gas or unperturbed chain conformations needed for the estimation of the segmental chemical potential were sampled using simple reptation moves.[23,35]

A major part of this work was devoted to the calculation of excess chain and segmental chemical potentials in the liquid and gas phases. As mentioned in section 3, in the bulk (liquid or gas), the inserted test molecule was grown segment by segment with configurational bias except for the first mer, which was placed at random. The numbers of trial values for the generalized coordinates were $N_{\psi_{12}} = 6$ to 9, $N_{\psi_3} = 6$ to 9, $N_{\theta_i} = 1$ ($1 \le i \le n_{test} - 2$), and $N_{\phi_i} = 6-9$ ($2 \le i \le n_{test} - 2$). In other words, $n_{trial} = 6-9$ trial positions were generated for each segment, the higher value being best for low-temperature, high-density phases. With the Smit *et al.* model, the single value of θ_i needed for each additional segment was picked from a distribution proportional to $\sin\theta \exp(-\beta U_{bending}(\theta))$. The single reference chains in continuous space were also grown segment by segment with configurational bias, except for the first three segments. $n_{trial} = 6$ proved sufficient for growing each segment beyond the third. Results for all values of n_{test} were obtained in parallel by inserting each time a *n*-hexane test molecule and progressively growing it to *n*-hexadecane. When an added segment experienced excessive steric overlaps with its environment at all n_{trial} positions tried, the growth procedure was terminated and contributions to μ^{ex} from the particular test chain insertion were taken into account only for n_{test} values up to that point. Similarly, in the estimation of μ^{ex}_{seg}, $N_{seg} = 6-9$ positions were tried for the appended segment.

In all cases, error bars are estimated using a standard block-averaging analysis.[2]

Table 2. Estimation of Densities and Solubility Parameters at $T = 580$ K[a]

pure component properties	Dodd and Theodorou model	Smit et al. model	Lee−Kesler correlation
ρ_{vapor} (g/cm^3)	0.005 ± 0.002	0.005 ± 0.002	0.005
ρ_{liquid} (g/cm^3)	0.56 ± 0.03	0.58 ± 0.03	0.55
δ (J/cm^3)$^{1/2}$	10.14	11.10	9.79

[a] The pressure for the vapor is $P = 1.02$ atm and for the liquid is $P = 50$ atm.

5. Results and Discussion

***PVT* Behavior, Structure, and Conformation.** The volumetric properties obtained from the *NPT* simulations of liquid and gas C_{16} are examined first. In Table 2, a comparison between densities obtained from simulations and from the Lee−Kesler correlation[29] at $T = 580$ K is shown. For all practical purposes, the Lee−Kesler predictions can be considered equivalent to experimental values. For the vapor phase, there is excellent agreement between simulation results from both molecular models and Lee−Kesler predictions. The Smit *et al.* model overpredicts the liquid density somewhat, while the Dodd and Theodorou model gives a very satisfactory estimate for this quantity.

The solubility parameter δ of the liquid was obtained as the square root of the cohesive energy density. The cohesive energy was estimated from the simulation as the mean total potential energy of intermolecular interactions, and from macroscopic thermodynamics as the energy of vaporization at the prevailing temperature. The agreement seen in the last line of Table 2 is satisfactory, especially for the Dodd and Theodorou model. At the lower temperature studied (450 K) the value of δ from this model is 12.38 (J/cm^3)$^{1/2}$ while the experimental is 12.47 (J/cm^3)$^{1/2}$. The solubility parameter increases with decreasing temperature. For comparison, the literature[29] value of δ for polyethylene at room temperature is 16.3 (J/cm^3)$^{1/2}$.

Figure 1 shows typical configurations of a gas (part a) and a liquid phase (part b) at $T = 580$ K. The structure of both phases is examined through the *inter*molecular pair distribution function $g(r)$ and the *intra*molecular pair density function $\omega(r)$. The intermolecular $g(r)$ for the gas is almost the same from both models, as shown in Figure 2. It exhibits a single broad peak and then drops to an asymptotic value of unity. The most probable distance between segments of different chains is approximately 6.2 Å, *i.e.* considerably larger than the van der Waals diameter of approximately 4.4 Å. In Figure 3 is shown the pair distribution function $g_{cm}(r)$ of the centers of mass of chains in the gas. The data exhibit considerable scatter because of the small number of centers of mass in the simulated system. The peak in $g_{cm}(r)$ is observed at a significantly higher separation (approximately 7.5 Å) than the peak in $g(r)$. This most probable separation between chain

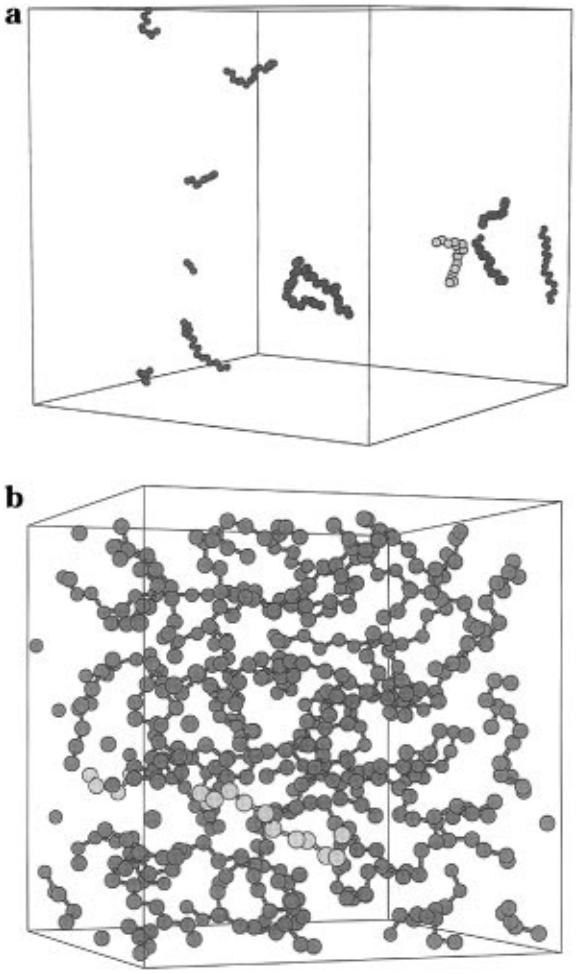

Figure 1. Typical configurations under vapor and liquid conditions of C_{16}: (a) gas at $T = 580$ K and $P = 1.02$ atm ($\rho = 0.005$ g/cm^3); (b) liquid at the same temperature and $P = 50$ atm ($\rho = 0.58$ g/cm^3). The inserted molecule is shown in lighter shading.

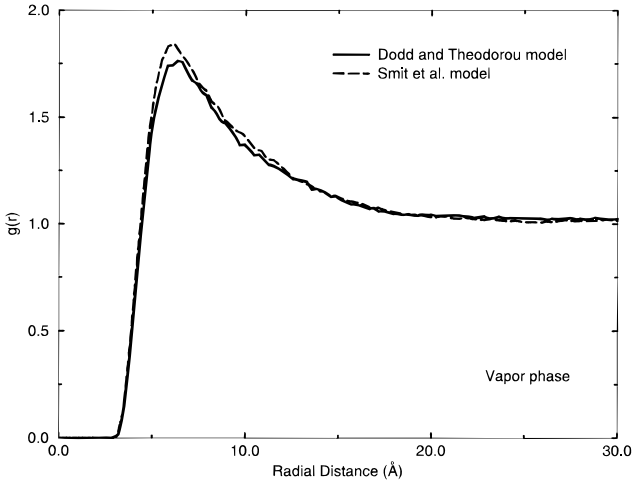

Figure 2. Interchain pair distribution function $g(r)$ in the gas phase. The curves obtained from both models at $T = 580$ K and $P = 1.02$ atm are almost identical.

centers of mass is commensurate to, but lower than, twice the root mean squared radius of gyration $\langle s^2 \rangle^{1/2}$ (see Tables 3 and 4). Also, the rise of $g_{cm}(r)$ at short distances is considerably more gradual that of $g(r)$, since chains, but not individual segments, can penetrate each other, to a certain extent. Thus, the structure of the vapor is somewhat more complex than would be expected from considering the alkane molecules as van der Waals spheres of diameter equal to $\langle s^2 \rangle^{1/2}$. The peaks in $g(r)$ and $g_{cm}(r)$ indicate a tendency for chains to form "dimers" under the conditions of the simulation, due to attractive intermolecular interactions. Such dimers can be seen below the center and on the right-hand side of the simulation box shown in Figure 1a.

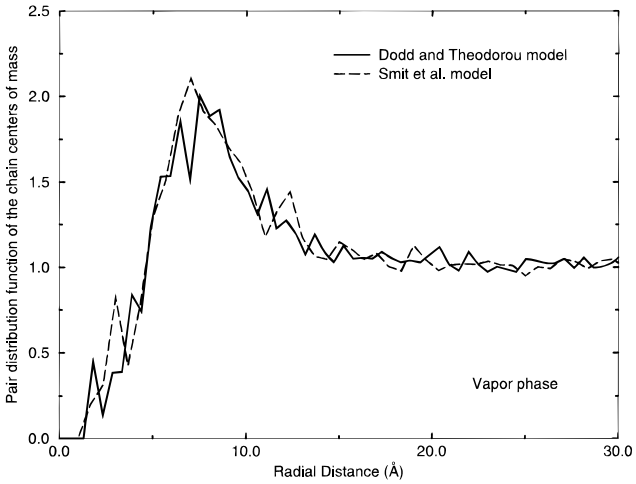

Figure 3. Pair distribution function of the chain centers of mass in the gas phase (580 K, 1.02 atm).

The intermolecular pair distribution function of the liquid is shown in Figure 4. The two models give practically identical $g(r)$ curves. The first coordination shell appears at a distance of approximately 5.9 Å. There are a second coordination shell and a hint of a third coordination shell. For distances up to the root mean squared end-to-end distance of chains (compare Tables 3 and 4) $g(r)$ appears considerably lower and less structured than the pair distribution function in a monomeric liquid in a corresponding thermodynamic state, because the neighborhood of a segment tends to be populated by segments of the same chain, which exclude segments of other chains. This is an instance of the well-known "correlation hole" effect.

The intra-chain pair density function $\omega(r)$ obtained in the bulk phase with the Smit *et al.* model is shown in Figure 5, along with $\omega(r)$ for continuous unperturbed chains governed by the same potential. The two functions are practically identical, indicating that chain conformations in the bulk liquid conform to Flory's "random coil hypothesis" down to atomic length scales. The corresponding results for the Dodd and Theodorou model are very similar to those obtained in the past[23] for C_{24} and will not be reproduced here; they, too, show excellent agreement between conformation in the bulk liquid and continuous unperturbed chain conformation.

The structure of the liquid phase was examined further through the k-weighted structure factor $k(S(k) - 1)$, as shown in Figure 6. The curve in Figure 6a is obtained through a Fourier transform of $g^{tot}(r) = g(r) + \omega(r)/\rho$ of the liquid when the Dodd and Theodorou model is used at $T = 450$ K. The experimental data are from X-ray measurements[37] for C_{15} at $T = 293$ K. In Figure 6b, simulation results are presented from the Smit *et al.* model at $T = 580$ K, along with experimental data[37] for C_{20} at $T = 315$ K. (Unfortunately, experimental data for n-alkanes at 450 and 580 K are not available in the literature.) In both cases, the location of the first (interchain) peak is captured very well by the simulation; its height, as well as that of the second peak, is lower than that in the experimental data, because the

Table 3. Conformational Properties Obtained from the Dodd and Theodorou Model at $T = 580$ K

conformational property	vapor	ideal gas	liquid	unperturbed chain	RIS predictions[40]
$\langle r^2\rangle$ (Å^2)	170.8 ± 0.9	170.4	180.1 ± 2.4	182.4	
$\langle s^2\rangle$ (Å^2)	21.29 ± 0.07	21.26	21.96 ± 0.15	22.14	
$\langle r^2\rangle_0/\langle s^2\rangle_0$			8.20 ± 0.02	8.24	8.01
$C_n = \langle r^2\rangle/nl^2$			5.06 ± 0.07	5.13	4.90
P_t	0.603	0.602	0.614	0.618	

Table 4. Conformational Properties Obtained from the Smit *et al.* Model at $T = 580$ K

conformational property	vapor	ideal gas	liquid	unperturbed chain	RIS predictions[40]
$\langle r^2\rangle$ (Å^2)	168.3 ± 0.9	166.4	178.2 ± 2.6	178.7	
$\langle s^2\rangle$ (Å^2)	21.27 ± 0.07	21.09	21.95 ± 0.18	21.98	
$\langle r^2\rangle_0/\langle s^2\rangle_0$			8.12 ± 0.02	8.13	8.01
$C_n = \langle r^2\rangle/nl^2$			5.01 ± 0.07	5.02	4.90
P_t	0.591	0.579	0.599	0.594	

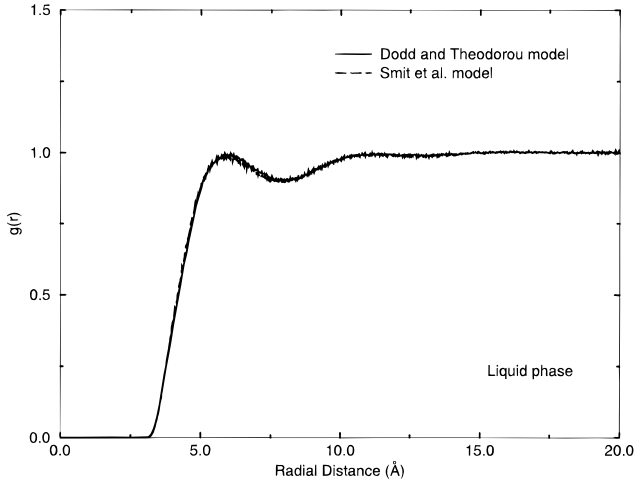

Figure 4. Interchain pair distribution function $g(r)$ in the liquid phase at $T = 580$ K and $P = 50$ atm. The two molecular models give indistinguishable results.

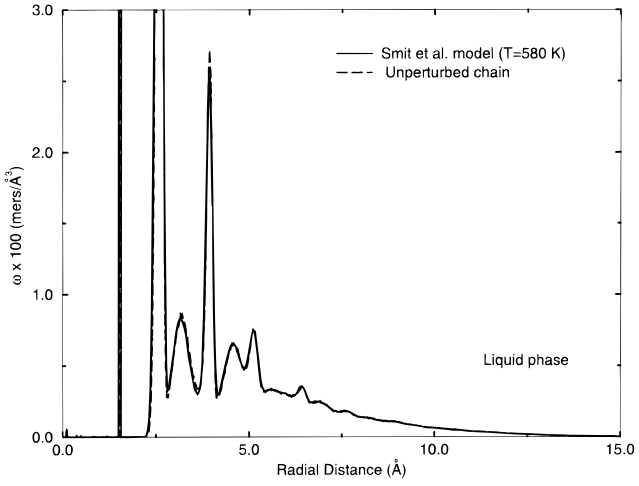

Figure 5. Intrachain pair density function $\omega(r)$ in the liquid phase (580 K, 50 atm). The molecular model of Smit *et al.* is used. The unperturbed chain results are also shown (dashed curve).

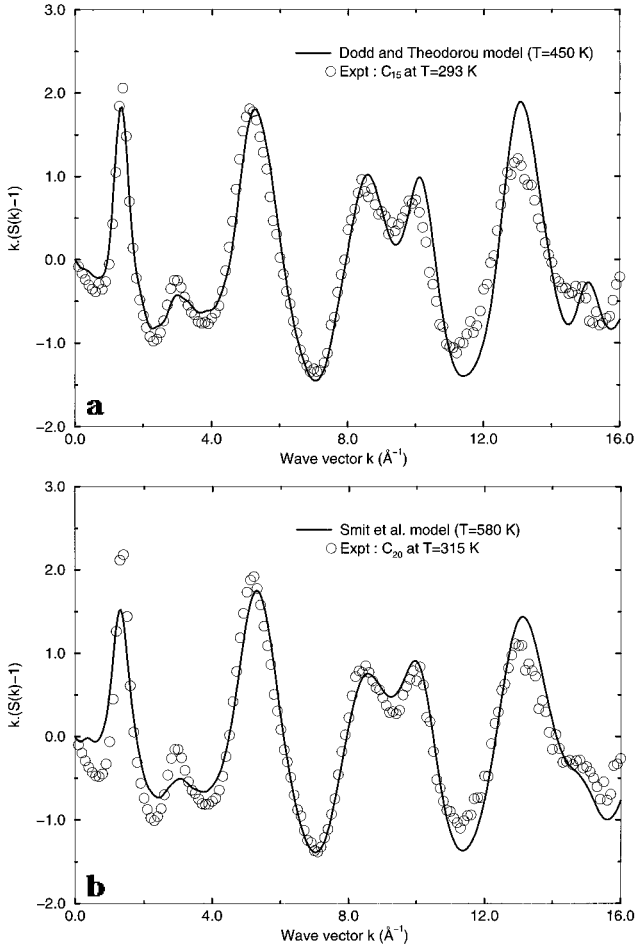

Figure 6. k-weighted structure factor: (a) simulation data for n-C_{16} obtained from the Dodd and Theodorou model at $T = 450$ K and $P = 20$ atm (circles: experimental data for C_{15} at $T = 293$ K); (b) simulation data from Smit *et al.* model at $T = 580$ K and $P = 50$ atm (circles: experimental data for C_{20} at $T = 315$ K).

temperature in the simulations is significantly higher than that in the measurements. Note that the predicted $S(k)$ below approximately 0.3 Å^{-1} is affected by discontinuities in the long-distance tail of $g(r)$, as accumulated in the periodic simulation box, and therefore any features appearing in this region are not meaningful. The bonded peaks at $k \geq 4$ Å^{-1} are not affected strongly by temperature, and therefore show very good agreement between simulation and experimental data. In contrast to the Dodd and Theodorou model (Figure 6a), the Smit *et al.* model allows for flexibility of the bond angles. As a result, it gives better agreement with the experimental data at high k values (short distances), where the Dodd and Theodorou model clearly overpredicts structure.

Conformational characteristics in the liquid and vapor phases, as well as in the reference ideal gas and unperturbed chain states, are given in Tables 3−5. The properties examined are the mean squared end-to-end distance $\langle r^2\rangle$, the mean squared radius of gyration $\langle s^2\rangle$, the characteristic ratio C_n ($=\langle r^2\rangle/nl^2$ with l equal to the bond length) of a chain with n bonds, and the probability of encountering a torsion angle in a *trans*

Table 5. Conformational Properties Obtained from the Dodd and Theodorou Model at $T = 450$ K

conformational property	liquid	unperturbed chain	RIS predictions[40]
$\langle r^2\rangle$ (Å^2)	192.5 ± 2.7	192.9	
$\langle s^2\rangle$ (Å^2)	22.95 ± 1.18	22.99	
$\langle r^2\rangle_0/\langle s^2\rangle_0$	8.38 ± 0.05	8.39	8.01
$C_n = \langle r^2\rangle/nl^2$	5.41 ± 0.08	5.42	4.90
P_t	0.652	0.653	

state, P_t. In Tables 3 and 5, results are shown for the molecular model of Dodd and Theodorou at two different temperatures (450 and 580 K). At the lower temperature, the simulation was performed only for the liquid phase; vapor conformational properties are very close to the ideal gas properties for both temperatures, and so there was no interest in simulating the low-temperature vapor phase. The data presented in Table 4 are obtained from the Smit *et al.* model at $T = 580$ K. The liquid conformational properties compare excellently with those of unperturbed chains, as expected from Flory's random coil hypothesis.[38] Interestingly, these and other simulation investigations we have conducted with realistic models indicate that the conformation of chains in the melt state is quite insensitive to the exact pressure (or density) for temperatures not too close to the critical point. The RIS[39] (rotational isomeric state) model predictions for unperturbed chains, given in the last column of these tables, are taken from Mattice and Suter[40] for polyethylene at room temperature. Clearly, chains in the ideal gas phase are more compact (lower $\langle r^2\rangle$, $\langle s^2\rangle$, and P_t) than unperturbed chains because of the additional nonlocal attractive interactions between segments more than four bonds apart, which are present in the ideal gas but absent in the unperturbed state.

The chains simulated with the Smit *et al.* model (Table 4) are slightly more compact than those simulated with the other model (Table 3). In the gas phase this is partly due to the increased attractions with chain ends (higher ϵ), which result in more contracted conformations. In the liquid and unperturbed chain states, the probability of *trans* for the Smit *et al.* model is lower because the torsional potential of Jorgensen used by Smit *et al.* has a broader *gauche*-state energy well than that of Ryckaert and Bellemans, used by Dodd and Theodorou. Comparing Tables 3 and 5, obtained with the same model at two different temperatures, we observe that, at the lower temperature, chains are more extended and a higher probability of *trans* is obtained. This is fully expected; at the lower temperature, the balance between conformational entropy and energy will shift toward lower energy, more extended conformations.

From the above discussion, it is evident that the MC simulations manage to equilibrate the overall conformational features of chains very well and that conformational predictions from both models in the gas and liquid phases are accurate and physically meaningful.

Excess Chemical Potential. An important aim of this work is to test the reliability of the chain increment method for estimating the chemical potential from detailed molecular models in both gas and liquid phases. In Figures 7 and 8, values of the excess chemical potential obtained from the two models for $n_{test} = 6-16$ are compared against EoS predictions. The reference state in all cases is the ideal gas. μ^{ex} varies linearly with the carbon number of the inserted molecule for the entire range of chain length both from simulation and from the cubic EoS. This is a proof that the incremental

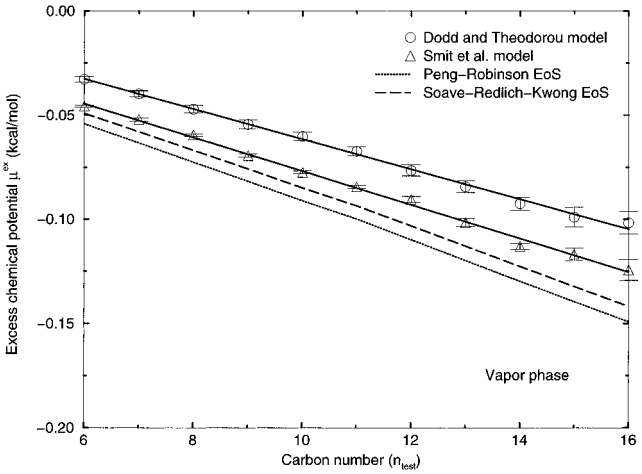

Figure 7. Excess chemical potential results vs carbon number in the gas phase (580 K, 1.02 atm) from the *NPT* Monte Carlo simulation. EoS predictions are shown for comparison.

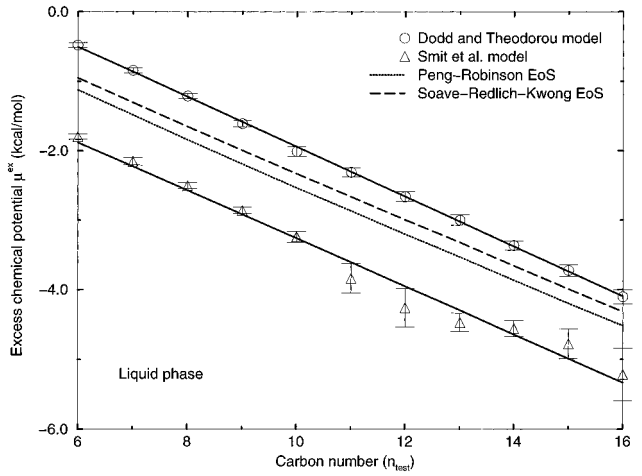

Figure 8. Excess chemical potential calculations in the liquid phase (580 K, 50 atm). The EoS predictions are shown for comparison.

Table 6. Excess Chemical Potential Calculations in the Vapor Phase at $T = 580$ K, from Molecular Simulation and EoS (All Values in kcal/mol)

vapor phase calculations	$d\mu^{ex}/dn_{test}$ (ref: ideal gas)	μ^{ex}_{seg} increm (ref: ideal gas)
Dodd and Theodorou model	−0.0072 ± 0.0002	−0.0079 ± 0.0008
Smit *et al.* model	−0.0081 ± 0.0001	−0.0095 ± 0.0004
Peng−Robinson EoS	−0.0095	
Soave−Redlich−Kwong EoS	−0.0093	

ansatz[5] is valid in both phases for the system studied. In the vapor phase, the Smit *et al.* model is closer to the EoS curves, while in the liquid phase results from the two molecular models and the EoS deviate significantly from each other. The Dodd and Theodorou model seems somewhat closer to the EoS predictions in the liquid.

In Tables 6 and 7, the slopes of the above $\mu^{ex}(n_{test})$ curves are compared against the EoS predictions for the segmental chemical potential μ^{ex}_{seg} computed by test segment insertions in the course of the simulations. The agreement is very good for both phases and molecular models.

For the liquid phase calculations, results were obtained for two reference states: the ideal gas and the continuous unperturbed chain. As shown in Figure 9, μ^{ex} still varies linearly with n_{test} when the unperturbed chain is used as a reference. The absolute value of the

Table 7. Excess Chemical Potential Calculations in the Liquid Phase at T = 580 K, from Molecular Simulation and EoS (All Values in kcal/mol)

liquid phase calculations	$d\mu^{ex}/dn_{test}$ (ref: ideal gas)	μ^{ex}_{seg} increm (ref: ideal gas)	$d\mu^{ex}/dn_{test}$ (ref: unpert chain)	μ^{ex}_{seg} increm (ref: unpert chain)
Dodd and Theodorou model	-0.362 ± 0.006	-0.363 ± 0.004	-0.439 ± 0.006	-0.449 ± 0.004
Smit *et al.* model	-0.357 ± 0.01	-0.354 ± 0.003	-0.430 ± 0.01	-0.436 ± 0.003
Peng−Robinson EoS	−0.339			
Soave−Redlich−Kwong EoS	−0.335			

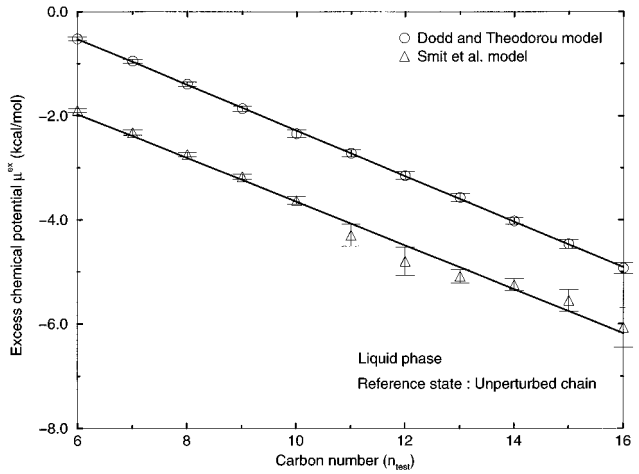

Figure 9. Excess chemical potential calculations in the liquid (580 K, 50 atm) using the continuous unperturbed chain as reference state. Both models predict linear behavior.

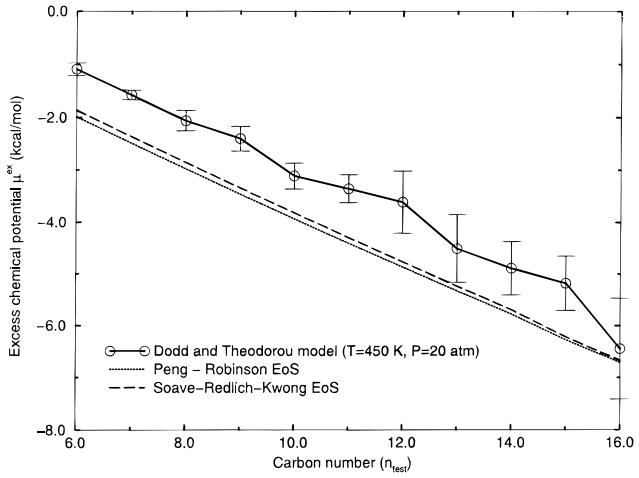

Figure 10. Excess chemical potential calculations in the liquid phase from simulation and from EoS at low temperature (450 K, 20 atm). Simulation results were obtained using the Dodd and Theodorou model.

segmental μ^{ex} is actually larger when the unperturbed chain is used as the reference state. This implies that there is no real advantage in using the unperturbed chain as reference for the liquid when phase equilibrium calculations are considered.

Our study of the liquid at 450 K ($T_r = T/T_c = 0.6$) was motivated by de Pablo *et al.*'s finding that the incremental ansatz is not satisfied[9] for a detailed atomistic model. (Their studies were conducted at $T_r = 0.6$). Our results for the excess chemical potential at 450 K and P = 20 atm, using the Dodd and Theodorou model, are presented in Figure 10. They indicate that configurational bias insertions of entire chains are difficult and unreliable under these conditions. The nonlinear variation of μ^{ex} with the length of the inserted molecule and the large error bars on the simulation points show that, even using CBMCI, the important configurations which shape the value of μ^{ex} are rarely sampled, especially for large n_{test}. On the contrary, the EoS-based values of μ^{ex}, presented in the same figure, show an almost perfectly linear variation with n_{test} at this temperature. On the basis of this observation, we are led to the conclusion that the chain increment ansatz, eq 1, is still valid at this low temperature. The deviation from linearity between μ^{ex} and n_{test} reported in ref 9 and the problems with our own simulation results in Figure 10 seem to have a numerical, rather than a physical origin, namely insufficient sampling of the relevant configurations by the inserted molecule at low temperature. In contrast to μ^{ex}, μ^{ex}_{seg} can still be calculated efficiently at low temperatures through test segment insertions. In this case, the calculated value for μ^{ex}_{seg} is -0.499 ± 0.009 kcal/mol, whereas the EoS slope is −0.48 kcal/mol. In addition, a straight line drawn through the simulation data of Figure 10 has a slope equal to -0.494 ± 0.031 kcal/mol. Thus, computing μ^{ex} for a small test molecule (e.g. $n_{small} = 6$) by CBMCI and μ^{ex}_{seg} by virtual augmentation of the matrix chains and then invoking the incremental ansatz, eq 1, seems to be the safest method for estimating μ^{ex} for large n at low temperatures.

6. Conclusions

In this work, Monte Carlo simulation and a realistic molecular representation were used to study the thermodynamic and structural properties of an oligomeric fluid (*n*-hexadecane) under liquid and vapor conditions at 580 K and of *n*-alkane chains of various lengths dissolved in it at infinite dilution. Two different molecular models were used to describe the intermolecular and intramolecular interactions in the system. Volumetric and structural properties were calculated in good agreement with experimental data. Two reference states were examined: a fluid of noninteracting continuous unperturbed chains and an ideal gas. Liquid phase conformational properties, such as the chain radius of gyration and the end-to-end distance, were in excellent agreement with the continuous unperturbed chain predictions for both molecular models, indicating that the system follows the random coil hypothesis. On the other hand, the vapor phase conformation resembled closely the ideal gas conformation.

A rigorous formulation was derived for the calculation of the excess chemical potential of chains (μ^{ex}) and of the excess segmental chemical potential (μ^{ex}_{seg}) from Monte Carlo simulation, using Widom insertions of chains and segments. The formulation was implemented using a configurational bias Monte Carlo integration strategy. At 580 K, μ^{ex} for a series of linear chains inserted in *n*-hexadecane varies linearly with the carbon number (n_{test}) of the chain for all chain lengths examined (from $n_{test} = 6$ up to $n_{test} = 16$) and for both phases. Results for μ^{ex}_{seg} based on equations of state that are known to describe experimental data for normal hydrocarbon mixtures accurately also exhibit this linearity. Therefore, the incremental chemical potential ansatz (eq 1) is shown to be valid, and the lowest chain

length examined here ($n_{small} = 6$) can be used as a basis in order to calculate μ^{ex} of longer chains.

For the liquid phase calculations, both reference states (continuous unperturbed chain and ideal gas) were used to obtain μ^{ex}, and in both cases μ^{ex} was found to vary linearly with n_{test}. On the basis of the calculations presented here, there is no apparent advantage in using the continuous unperturbed chain as a reference state for the liquid phase.

Monte Carlo simulation was performed at a lower temperature (450 K) in order to examine the validity of our conclusions under such conditions. Although volumetric and structural property predictions are again in good agreement with experimental data, Widom insertions are plagued by poor sampling, and therefore the estimates of the chain chemical potential from simulations are inaccurate. Nevertheless, based on equation of state calculations, one expects that the excess chemical potential would still vary linearly with n_{test}, and thus the incremental ansatz would be valid.

Based on the comparisons presented above, we expect that the molecular models examined here, in conjunction with the chain increment ansatz, should be able to predict with reasonable accuracy the phase equilibria of heavy hydrocarbons and hydrocarbon/linear polyethylene systems. Currently, the validity of these models and methods for direct calculation of mixture phase equilibria is examined.

Acknowledgment. We are indebted to Dr. Vlasis Mavrantzas for his help with programming and for making his polyethylene simulation code available to us. Stimulating discussions with Professor Thanasis Panagiotopoulos are deeply appreciated. D.N.T. thanks the Institute for Theoretical Physics at the University of California, Santa Barbara, CA, for its hospitality during the last stage of this work; partial support for this visit was provided by the National Science Foundation under Grant No. PHY94-07194.

References and Notes

(1) Colbourn, E. A., Ed. *Computer Simulation of Polymers*; Longman Publishers: Essex, U.K., 1994.
(2) Allen, M. P.; Tildesley, D. J. *Computer Simulation of Liquids*; Oxford University Press: London, 1987.
(3) Panagiotopoulos, A. Z. In *Supercritical Fluids. Fundamentals for Application*; Kiran, E., Levelt Sengers, J. M. H., Eds.; Kluwer Academic Publishers: Dordrecht, The Netherlands, 1994.
(4) Panagiotopoulos, A. Z. *Mol. Phys.* **1987**, *61*, 813.
(5) Kumar, S. K.; Szleifer, I.; Panagiotopoulos, A. Z. *Phys. Rev. Lett.* **1991**, *66*, 2935.
(6) Widom, B. *J. Chem. Phys.* **1963**, *39*, 2808.
(7) Sheng, Y. J.; Panagiotopoulos, A. Z.; Kumar, S. K; Szleifer, I. *Macromolecules* **1994**, *27*, 400.
(8) Kacker, N.; Weinhold, J. D.; Kumar, S. K. *J. Chem. Soc., Faraday Trans.* **1995**, *91*, 2457.
(9) de Pablo, J. J.; Laso, M.; Suter, U. W. *J. Phys. Chem.* **1992**, *96*, 6157.
(10) Sheng, Y.-J.; Panagiotopoulos, A. Z. *Macromolecules* **1996**, *29*, 4444.
(11) Escobedo, F. A.; de Pablo, J. J. *J. Chem. Phys.* **1995**, *103*, 2703.
(12) Müller, M.; Paul, W. *J. Chem. Phys.* **1994**, *100*, 719.
(13) Wilding, N. B.; Müller, M. *J. Chem. Phys.* **1994**, *101*, 4324.
(14) Wolfgardt, M.; Baschnagel, J.; Binder, K. *J. Chem. Phys.* **1995**, *103*, 7166.
(15) Dickman, R.; Hall, C. K. *J. Chem. Phys.* **1986**, *85*, 4108.
(16) Honnell, K. G.; Hall, C. K. *J. Chem. Phys.* **1989**, *90*, 1841.
(17) Chapman, W. G.; Gubbins, K. E.; Jackson, G.; Radosz, M. *Ind. Eng. Chem. Res.* **1990**, *29*, 1709.
(18) Wertheim, M. S. *J. Stat. Phys.* **1984**, *35*, 19.
(19) Wertheim, M. S. *J. Stat. Phys.* **1986**, *42*, 459.
(20) Chen, S. J.; Economou, I. G.; Radosz, M. *Macromolecules* **1992**, *25*, 3089.
(21) Banaszak, M.; Chen, C. K.; Radosz, M. *Macromolecules* **1996**, *29*, 6481.
(22) Song, Y.; Lambert, S. M.; Prausnitz, J. M. *Ind. Eng. Chem. Res.* **1994**, *33*, 1047.
(23) Dodd, L. R.; Theodorou, D. N. *Adv. Pol. Sci.* **1994**, *116*, 249.
(24) Smit, B.; Karaborni, S.; Siepmann, J. I. *J. Chem. Phys.* **1995**, *102*, 2126.
(25) Theodorou, D. N.; Suter, U. W. *Macromolecules* **1985**, *18*, 1467.
(26) Maginn, E. J.; Bell, A. T.; Theodorou, D. N. *J. Phys. Chem.* **1995**, *99*, 2057.
(27) Prausnitz, J. M.; Lichtenthaler, R. N.; Azevedo, E. G. *Molecular Thermodynamics of Fluid-Phase Equilibria*, 2nd ed.; Academic Press: New York, 1986.
(28) Walas, S. M. *Phase Equilibria in Chemical Engineering*; Butterworth Publishers: Stoneham, MA, 1985.
(29) Reid, R. C.; Prausnitz, J. M.; Poling, B. E. *The Properties of Gases and Liquids*, 4th ed.; McGraw-Hill: New York, 1987.
(30) Ambrose, D.; Tsonopoulos, C. *J. Chem. Eng. Data* **1995**, *40*, 531.
(31) Theodorou, D. N.; Boone, T. D.; Dodd, L. R.; Mansfield, K. F. *Makromol. Chem. Theory Simul.* **1992**, *2*, 191.
(32) Frenkel, D.; Smit, B. *Mol. Phys.* **1991**, *75*, 983.
(33) Frenkel, D.; Mooij, G. C. A. M.; Smit, B. *J. Phys.: Condens. Matter* **1992**, *3*, 3053.
(34) Siepmann, J. I.; Frenkel, D. *Molec. Phys.* **1992**, *75*, 59.
(35) Pant, P. V. K; Theodorou, D. N. *Macromolecules* **1995**, *28*, 7224.
(36) Dodd, L. R.; Boone, T. D.; Theodorou, D. N. *Mol. Phys.* **1993**, *78*, 961.
(37) Habenschuss, A.; Narten, A. H. *J. Chem. Phys.* **1990**, *92*, 5692.
(38) Flory, P. J. *Principles of Polymer Chemistry*; Cornell University Press: Ithaca, NY, 1953.
(39) Flory, P. J. *Statistical Mechanics of Chain Molecules*; Wiley: New York, 1969.
(40) Mattice, W. L.; Suter, U. W. *Conformational Theory of Large Molecules*; Wiley: New York, 1994.

MA970178E